

GEOMETRIC CORRECTION OF ADEOS-II/GLI

Toshiaki HASHIMOTO

Center for Environmental Remote Sensing (CEReS), Chiba University, Japan
hashi@ceres.cr.chiba-u.ac.jp

Working Group I/5

KEY WORDS: Algorithms, Mapping, Sensors, Orientation

ABSTRACT

The GLI (Global Imager) on board the ADEOS-II is an optical mechanical scanner with 36 channels and the spatial resolution of 1 km and 250m at nadir. It is the successor of the ADEOS/OCTS (Ocean Color and Temperature Scanner) and observed the Earth surface only in daytime. The author is one of the PIs (principal investigators) and in the charge of precise geometric correction of the GLI. This paper describes the main characteristics of the GLI, the methodology of geometric correction and some products.

1 INTRODUCTION

The ADEOS-II (Advanced Earth Observing Satellite-II) has being developed and will be launched in 2001 by National Space Development Agency of Japan (NASDA). The main mission of ADEOS-II is summarized in three points: to monitor regularly the water and energy cycle in the global climate system, to estimate quantitatively the biomass and fundamental productivity in the carbon cycle, to detect the signal of long term climate changes. To realize the mission objective, it is equipped with five sensors: the Global Imager (GLI), the Advanced Microwave Scanning Radiometer (AMSR), the Improved Limb Atmospheric Sounder-II (ILAS-II), the SeaWinds and the Polarization and Directionality of the Earth's Reflectance (POLDER).

The GLI is an optical mechanical scanner with 36 channels. It is the successor of the OCTS on board the ADEOS and very similar to EOS-Terra/MODIS. It is designed for four kinds of application fields like atmosphere, ocean, land and cryosphere. In the field of land application, the geometric accuracy is very important because of multi-temporal analysis, image composite.

The initial checks of ADEOS data indicated that the geometric accuracy of the OCTS imagery was about 10 pixels. NASDA and some organization examined the factors for such terrible errors and found out three factors; 1) the bug of the software for determining satellite position, 2) the insufficiency of the algorithm for getting satellite attitude, 3) the miss-alignments of the sensors. Among them, the first factor was easy to fix. With respect to the second one, a new algorithm adopted to the ADEOS-II satellite has been examined. The third one was corrected using a number of ground control points (GCP) from many OCTS images. The modification of processing system at the ground station lead to the geometric accuracy of the OCTS imagery within a few pixels.

Some factors of the ADEOS-II concerning geometric accuracy will be improved rather than those of the ADEOS. For example, a differential GPS system and a star sensor will be equipped in order to achieve accurate satellite position, to monitor satellite attitude, respectively. It will be probable that the geometric accuracy of the GLI will be not sufficient in spite of such improvements.

If the satellite position and attitude are sufficiently accurate and the sensor alignments do not change after the launch, systematic geometric correction would achieve the sufficient accuracy. However, the experiences of the ADEOS/OCTS will indicate that the satellite attitude will not be so precise and the sensor alignments may change after the launch. NASDA is preparing the precise geometric correction system utilizing GCPs in case of insufficient geometric accuracy. In the system, such uncertain parameters as the satellite attitude and the miss sensor alignment are corrected on the basis of collinearly condition of photogrammetry.

The sensor alignments will be corrected during initial check out period. The geometric correction system in the normal operation is as follows. The GCPs are extracted automatically by image matching of coastal lines. The precise satellite position and attitude are determined using the GCPs. A rectified image is generated using the newly determined

satellite position and attitude. Mapping projection is Latitude/Longitude projection for low and middle latitude regions and Polar Stereo Projection for high latitude regions.

2 OVERVIEW OF GLI

2.1 Characteristics of GLI

The orbit of ADEOS-II satellite summarized in Table 1 is very similar to that of ADEOS except the recurrent period. It is just four days and any point on the earth can be observed three times in four days at least. Main characteristics of the GLI are shown in Table 2. The spectral range covers visible (VIS), near infrared (NIR), short wavelength infrared (SWIR), mid and thermal infrared (MTIR) regions. Two kinds of ground resolution are adopted; 1km and 250m. The spectral channels of the 250m channels are almost same as those of Landsat/TM. The GLI is often compared with the MODIS which has also 36 spectral channels. The former has 7 channels in MTIR, while the latter has 16 channels. It means that major observation targets are the ocean for GLI and the atmosphere and ground for MODIS. As same as the OCTS, the GLI has the tilt function for preventing sun-glitter, however, the sensor will not be tilted for land purpose. In other words, normally the GLI will observe the ocean with the tilt and the land without the tilt.

item	values
Type	sun synchronous, sub-recurrent
Period	101 min.
Altitude	803 km
Inclination	98.6 deg.
Recurrent period	4 days
Local time at descending node	AM.10:30±15min

Table 1 Main characteristics of orbit

item	values
spectral channels (for land)	VIS 1km : 13 (4), 250m : 3 (3)
	NIR 1km : 6 (3), 250m : 1 (1)
	SWIR 1km : 4 (2), 250m : 2 (2)
	MTIR 1km : 7 (3)
resolution at nadir	1 km, 250 m
swath angle	± 45 deg.
tilt angle	-20 deg., 0 deg., 20 deg.
quantization bits	12 bits/data

Table 2 Main characteristics of GLI

2.2 Land products

The raw data will be processed to make the Level 1B product of which the registration error and the radiometric distortion are corrected. The process of generating the products for land application start with Level 1B product as shown in Figure 1. Firstly the Level 1B product is geometrically corrected. This process is the subject of this paper. After the process, the data shown in Table 3 are generated. The composite of the geometrically corrected images in 16 days is generated for cloud screening. The criterion for determining which pixels is selected in the composite image is the degree of the cloudiness proposed by another PI. The atmospheric correction is applied to all channels except thermal channels of the composite. This product is called as 'L2A_LC'. The products like land covers, biomass, etc. are generated using the L2A_LC products.

data type	bytes/data
image data (all land channels)	2
scan geometry solar zenith angle, solar azimuth angle, satellite zenith angle, satellite azimuth angle	4
observation time	8
cloud flag	4
land/ocean flag	1
elevation (only 250m products)	2

Table 3 The summary of geometrically corrected data

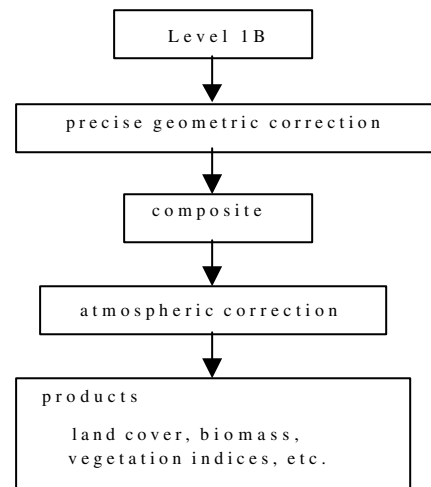


Figure 1. process flow for land products

3 METHODOLOGY OF GEOMETRIC CORRECTION

3.1 Collinearity equation

First of all, the coordinates systems used here are defined as follows ;

- (X,Y,Z): ECR(Earth Center Rotation) coordinates where the origin is the gravity center of the Earth, X axis is Greenwich Meridian at the equator, Z axis is North along the spin axis, Y is defined by right-handed rotation,
- (x, y, z): Orbital Coordinates where the origin is the gravity center of the satellite, z axis is nadir, y axis is defined by the outer product of z axis and velocity vector, x is defined by right-handed rotation.

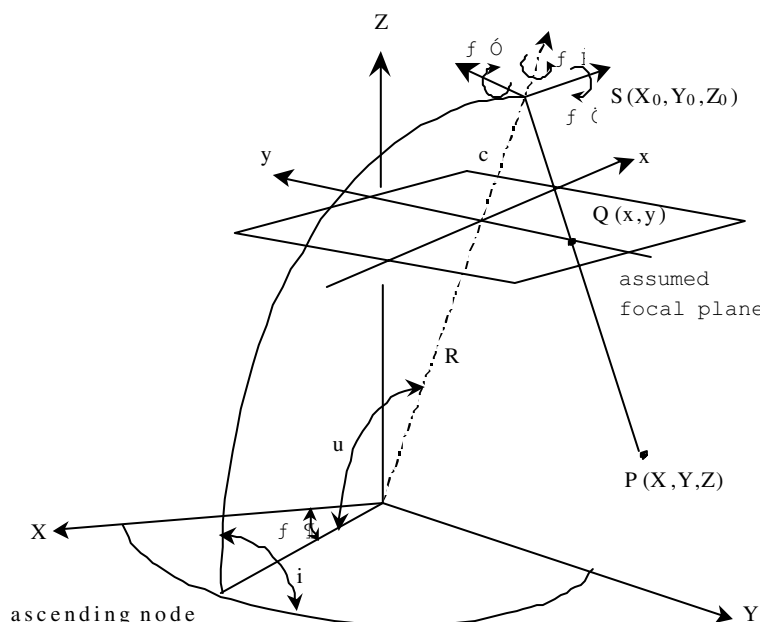


Figure 2. Collinearity condition

The view vector at the aperture (corresponding to the satellite coordinates) can be defined by the optical-mechanical system of GLI as (Bx_s, By_s, Bz_s) . The view vector in the coordinates are transformed into the orbital coordinates using the attitude, (roll, pitch, yaw) = $(\hat{u}, \hat{o}, \hat{e})$, as follows.

$$\begin{pmatrix} Bx_e \\ By_e \\ Bz_e \end{pmatrix} = \mathbf{P}_1 \cdot \begin{pmatrix} Bx_s \\ By_s \\ Bz_s \end{pmatrix} = \begin{pmatrix} \cos f \hat{e} & -\sin f \hat{e} & 0 \\ \sin f \hat{e} & \cos f \hat{e} & 0 \\ 0 & 0 & 1 \end{pmatrix} \begin{pmatrix} \cos f \hat{o} & 0 & \sin f \hat{o} \\ 0 & 1 & 0 \\ -\sin f \hat{o} & 0 & \cos f \hat{o} \end{pmatrix} \begin{pmatrix} 1 & 0 & 0 \\ 0 & \cos f \hat{o} & -\sin f \hat{o} \\ 0 & \sin f \hat{o} & \cos f \hat{o} \end{pmatrix} \begin{pmatrix} Bx_s \\ By_s \\ Bz_s \end{pmatrix} \tag{1}$$

where $e (Bx_s, By_s, Bz_s)$: view vector in satellite coordinates
 (Bx_e, By_e, Bz_e) : view vector in orbital coordinates.

The level 1B1 products contain the satellite position $\mathbf{P}_s = (X_o, Y_o, Z_o)$ and velocity $\mathbf{V}_s = (V_{xr}, V_{yr}, V_{zr})$ in ECR. The transformation between orbital coordinates and ECR coordinates is expressed as follows (NOAA/NESDIS), (Patt, F.S., et al, 1994), (Rosborough,G.W., et al, 1994).

let $\mathbf{n} = (x_e, y_e, z_e)$ F unit vector of \mathbf{P}_s , $\mathbf{u} = (u_x, u_y, u_z)$ F unit vector of \mathbf{V}_s ,

$$\text{then, } \begin{pmatrix} X_r \\ Y_r \\ Z_r \end{pmatrix} = \mathbf{P}_2 \cdot \begin{pmatrix} X_e \\ Y_e \\ Z_e \end{pmatrix} = \begin{pmatrix} x_k & x_m & x_n \\ y_k & y_m & y_n \\ z_k & z_m & z_n \end{pmatrix} \begin{pmatrix} X_e \\ Y_e \\ Z_e \end{pmatrix} \tag{2}$$

where (X_r, Y_r, Z_r) : any vector in ECR
 (X_e, Y_e, Z_e) : any vector in orbital coordinate s
 $\mathbf{m} = \mathbf{n} \times \mathbf{u} = (x_m, y_m, z_m)$: direction l vector for Y_e axis (in ECR)
 $\mathbf{k} = \mathbf{m} \times \mathbf{n} = (x_k, y_k, z_k)$: direction l vector for X_e axis (in ECR)

The satellite movement can be also expressed using the distance between the Earth center and the satellite center (R), the longitude of ascending node(\hat{U}), the inclination(i), the latitude argument from ascending node on the orbital plane(u) as follows (Hashimoto, T., 1998).

$$\begin{pmatrix} X_r \\ Y_r \\ Z_r \end{pmatrix} = \mathbf{P}_3 \cdot \begin{pmatrix} X_e \\ Y_e \\ Z_e \end{pmatrix} = \begin{pmatrix} \cos \Omega & \sin \Omega & 0 \\ \sin \Omega & -\cos \Omega & 0 \\ 0 & 0 & 1 \end{pmatrix} \begin{pmatrix} 1 & 0 & 0 \\ 0 & \sin i & -\cos i \\ 0 & \cos i & \sin i \end{pmatrix} \begin{pmatrix} -\sin u & 0 & \cos u \\ 0 & 1 & 0 \\ \cos u & 0 & \sin u \end{pmatrix} \begin{pmatrix} X_e \\ Y_e \\ Z_e \end{pmatrix} \quad (3)$$

$$= \begin{pmatrix} -\cos \Omega \sin u - \sin \Omega \cos i \cos u & \sin \Omega \sin i & \cos \Omega \cos u - \sin \Omega \cos i \sin u \\ -\sin \Omega \sin u + \cos \Omega \cos i \cos u & -\cos \Omega \sin i & \sin \Omega \cos u + \cos \Omega \cos i \sin u \\ \sin i \cos u & \cos i & \sin i \sin u \end{pmatrix} \begin{pmatrix} X_e \\ Y_e \\ Z_e \end{pmatrix}$$

Both $(\mathbf{P}_s, \mathbf{V}_s)$ and (R, \hat{U}, i, u) are time dependent. The variation ratios of the former are bigger than those of the latter, especially at the equator or the polar regions. So the latter is suitable for the expression of satellite movement. In this work, the parameters for satellite movement and attitude are expressed by the polynomials of line number (L) as ;

$$\mathbf{P} = \mathbf{P}_0 + \mathbf{P}_1 \cdot L + \mathbf{P}_2 \cdot L^2 + \dots, \quad \mathbf{P} = (R, \Omega, i, u, w, f, k). \quad (4)$$

The coefficients of polynomials for (R, \hat{U}, i, u) and attitude are determined by the regression analysis using the satellite movement(position, velocity) and attitude in a standard product, respectively

The view vector and the observed ground point (X, Y, Z) satisfies the collinearity equations as follows (Hashimoto, T., 1992), (Hashimoto, T., 1997).

$$F_x = -\frac{Bx_s}{Bz_s} - c \cdot \frac{a_1(X - X_0) + a_2(Y - Y_0) + a_3(Z - Z_0)}{a_7(X - X_0) + a_8(Y - Y_0) + a_9(Z - Z_0)} = 0$$

$$F_y = -\frac{By_s}{Bz_s} - c \cdot \frac{a_4(X - X_0) + a_5(Y - Y_0) + a_6(Z - Z_0)}{a_7(X - X_0) + a_8(Y - Y_0) + a_9(Z - Z_0)} = 0 \quad (5)$$

where $\begin{pmatrix} a_1 & a_2 & a_3 \\ a_4 & a_5 & a_6 \\ a_7 & a_8 & a_9 \end{pmatrix} = (\mathbf{P}_3 \cdot \mathbf{P}_1)^T = \mathbf{P}_1^T \cdot \mathbf{P}_3^T, \quad c : \text{assumed focal length.}$

$$\begin{pmatrix} X_0 \\ Y_0 \\ Z_0 \end{pmatrix} = \begin{pmatrix} \cos \Omega \cos u - \sin \Omega \cos i \sin u \\ \sin \Omega \cos u + \cos \Omega \cos i \sin u \\ \sin i \sin u \end{pmatrix} \cdot R$$

In the equation (5), the parameters (R, \hat{U}, i, u) and $(\hat{u}, \hat{o}, \hat{e})$ are treated as exterior orientation parameters. If the observed satellite position is accurate and the unknown parameters are only satellite attitude, the equation (5) can be approximated by Taylor development around the unknown parameters as;

$$F_x^0 + \hat{f}_x - \frac{\partial F_x}{\partial \hat{u}} d\hat{u} - \frac{\partial F_x}{\partial \hat{f}} d\hat{f} - \frac{\partial F_x}{\partial \hat{e}} d\hat{e} = 0$$

$$F_y^0 + \hat{f}_y - \frac{\partial F_y}{\partial \hat{u}} d\hat{u} - \frac{\partial F_y}{\partial \hat{f}} d\hat{f} - \frac{\partial F_y}{\partial \hat{e}} d\hat{e} = 0 \quad (6)$$

where the notation ‘ 0 ’ means the approximation and (v_x, v_y) is residuals.

3.2 GCP collection

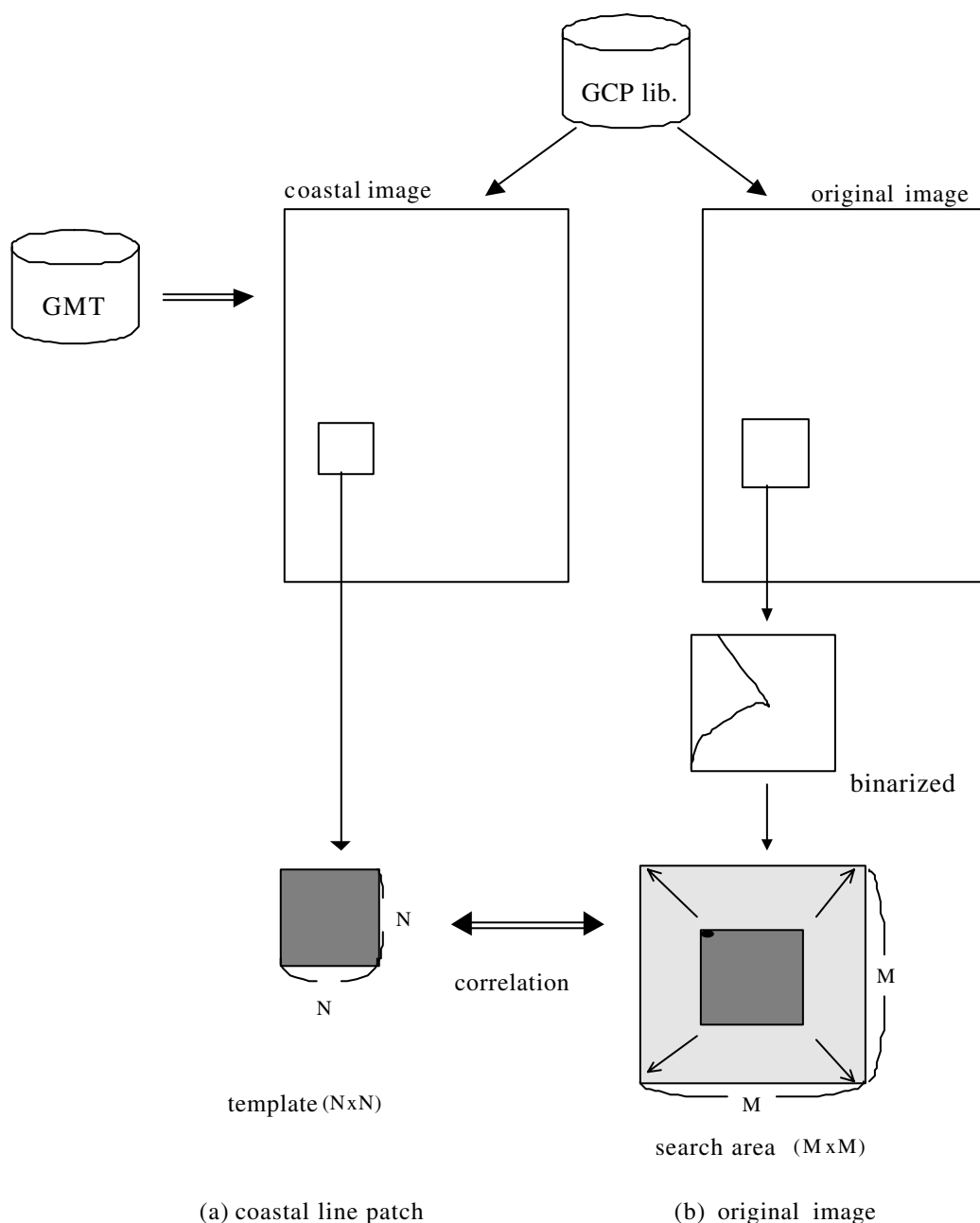


Figure 3. Procedure for GCP collection

Sufficient numbers of GCPs are necessary for exterior orientation. Conventionally, the GCP collection has been conducted by human interpretation. Such procedure is very time consuming and not proper for daily process. In this work, the GCP collection is realized by the template matching.

In figure 3, two image patches contain coastal lines. One (a) is a template from the Generic Mapping Tool (GMT) coastal data (Wessel, P.) prepared in advance, another (b) is a reference image made by the binarization of the original image. The template (a) is selected as a GCP candidate from the GCP library which have to be prepared. In this work, the sizes of both patches are determined as $m=32$ and $n=16$ through some experiments.

One scene of the GLI Level 1B1 data consists of 1656 lines and 1236 pixels for 1km product. But the GCP collection and the exterior orientation are carried out on the tilt segment basis because the orientation parameters are stable during the same tilt angle and more GCPs will be expected from one tilt segment than from one scene.

3.3 Map Projection

In the work, two kinds of projection methods are adopted, Latitude/Longitude projection for middle and low latitude regions (60°N - 60°S) and Polar Stereo projection for polar regions (90°N - 50°N, 50°S - 90°S). A whole projected area is divided into 56 sub-areas shown in Figure 3. The sub-area is a scene unit for ftp. One sub-area for the 1km products has the dimension of (3,800L x 3,600P) for Latitude/Longitude projection and (5,005L x 5,005P) for Polar Stereo projection, respectively. The map projection will be carried out scene by scene.

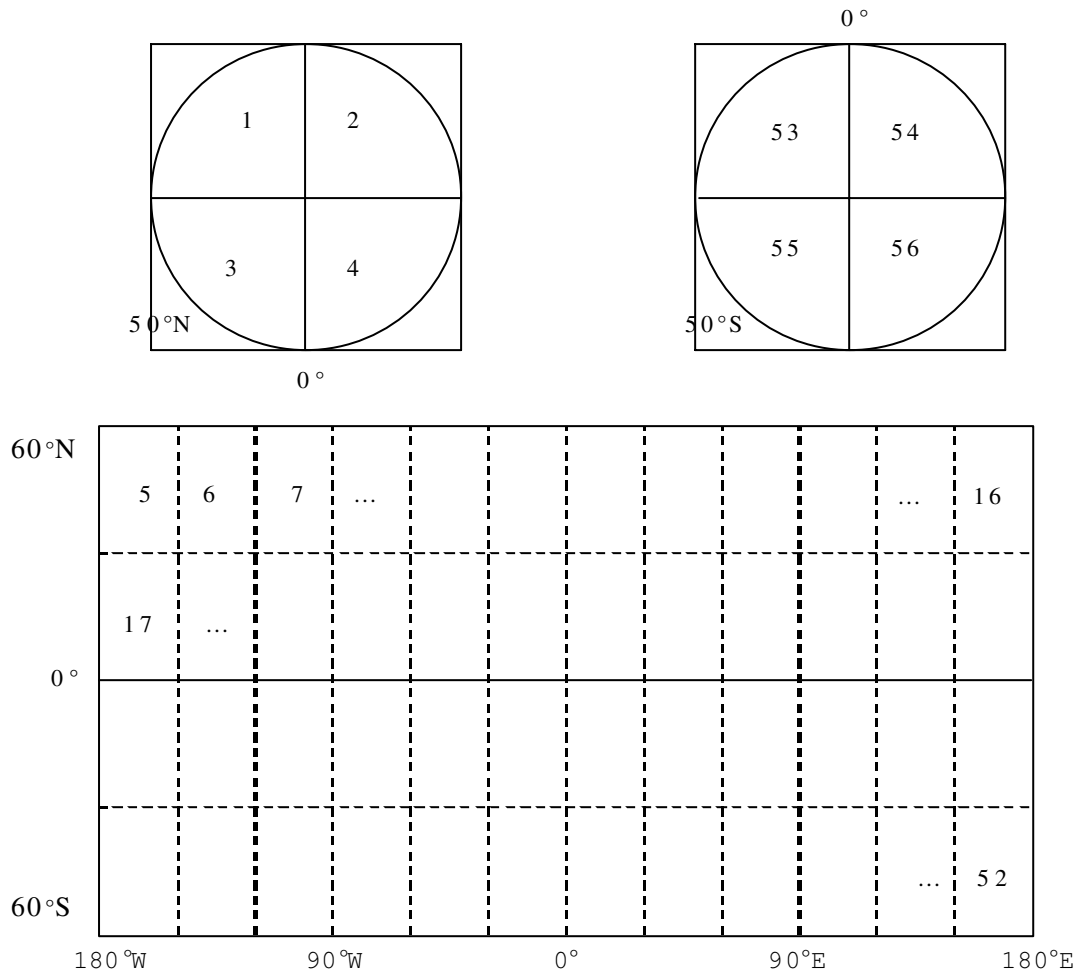


Figure 3. Sub areas for map projection

3.4 Correction of Sensor Alignment

During the initial check out period, the geometric accuracy will be examined with respect to the satellite position, the satellite attitude and the sensor alignment. If it will be found out that the sensor alignment was changed after the launch, the alignment should be corrected. The sensor alignment can be also corrected on the basis of collinearity condition (Hashimoto, H., 1999). In the equation (5), the view vector will be slightly changed by the alignment. The changes are specified by the optical system of the sensor. The equation (5) is linearized around the unknown parameters, or the alignment.

4 EXPERIMENTS

The actual GLI image is not yet available, off coarse. To examine the algorithm for geometric correction, the simulated data were generated from the OCTS data which observed around Japan. The orbit of the ADEOS was absolutely used as that of the ADEOS-II. The OCTS image was re-sampled to fit the resolution, the sampling ratio and the optical system of the GLI.

The method described in chapter 3 was examined utilizing the simulated data. It was proved that the system worked well. Concerning the GCP collection, sufficient number of GCPs could be obtained with good accuracy. But the accuracy of exterior orientation using the obtained GCPs was about 5 pixels, which was not precise. This was owing to that the scan geometry of GLI is very different from that of OCTS and the simulated image data could not reflect the actual condition of the GLI image. However, it is expected through the experiences of the system for AVHRR and OCTS that the geometric accuracy with less than one pixel for the GLI will be achieved.

5 CONCLUSIONS

The system for the precise geometric correction of ADEOS-II/GLI was developed. The algorithm of the geometric correction is based on the principle of collinearity condition. The experiment using the simulated data from OCTS data proved that the system worked well. To make the system applicable to actual GLI data, the following investigations have to be conducted.

- (1) NASDA has the plan to make some simulated data from the MODIS data. The check should be carried out how the system will work using the simulated data.
- (2) The sensor alignments are not considered in the current system. They will be applied to the system just after the ground measurement of them. Furthermore, if the change of the sensor alignment owing to the launch will be recognized during the initial check out period, they will be corrected using a huge number of GCPs from many images.
- (3) The spectral channels of GLI are different from those of OCTS. It should be investigated, using the simulated data from the MODIS data and the actual GLI data, which channel of GLI is suitable for obtaining coastal image data at the stage of GCP collection. The product of the GLI includes the land/ocean flag data which is also generated from the GMT. If they can be used as the coastal image patches, the process of the GCP collection will be easier to make the patches. The suitability of the land/ocean flag data for the GCP collection should be investigated using the actual GLI data.

REFERENCES

- Hashimoto, H., *et al*, 1992. Fast and Accurate Geometric Correction of NOAA AVHRR Imagery, Archives of 17th ISPRS, pp. 445-450.
- Hashimoto, H., 1997. Precise Geometric Correction of ADEOS/OCTS Imagery, Journal of JSPRS, Vol.36, No.5, pp.42-51.
- Hashimoto, H., 1998. The Estimation of Motion and Attitude of ADEOS Satellite Utilizing the Principle of Exterior Orientation, Journal of JSPRS, Vol.37, No.6, pp.4-13.
- Hashimoto, H., 1999. Correction of OCTS Sensor Alignment, Proc. of 20th ACRS, pp.807-811.
- NOAA/NESDIS, NOAA KLM User's Guide : Appendix I, on <http://www2.ncdc.noaa.gov/docs/klm/html/i/app-i.htm>
- Patt, F. S., *et al*, 1994. Exact closed-form geolocation algorithm for Earth survey sensors, Int'l Journal of Remote Sensing, Vol.15, No.18, pp.3719-3734.
- Rosborough, G. W., *et al*, 1994. Precise AVHRR Image Navigation, IEEE Trans. On Geoscience and Remote Sensing, Vol.32, No.3, pp.644-657.
- Wessel, P., GMT – The generic Mapping Tools, on <http://www.soest.hawaii.edu/gmt>